15

Synthesis of Novel Materials by Laser Rapid Solidification

E. J. Liang, J. Zhang and M. J. Chao
Zhengzhou University
China

1. Introduction

High power lasers have been widely used in industry as well as in laboratory for materials surface heat treatment, cladding, welding, cutting, thin film deposition by laser ablation and so on (Bogue, 2010; Chao & Liang, 2004; Wang et al., 2008; Kruusing, 2004), but they are seldom used in the synthesis of pure bulk materials. In recent years, we explored the synthesis of pure bulk materials with a high power CO_2 laser (Liang et al., 2007; 2007; 2008; 2009; Zhang et al., 2010). It is shown that a variety of materials can be successfully synthesized by laser rapid solidification (LRS). The materials synthesized by LRS exhibit unique microstructures, superior properties which may not be realized by traditional synthetic methods. Compared to the commonly used solid state reactions and wet chemical routes which are usually severe time and energy wasting or require expensive precursors, the laser synthetic technique provides a new and rapid method for the production of materials, with which tens of grams of a sample can be produced in a few or tens of seconds. In this paper we address the synthesis and characteristics of negative thermal expansion materials and ionic conductive materials using LRS. Particular attention will be paid to the unique microstructures, special or controlled phase formation and related superior properties of the materials synthesized by LRS which may not be obtained by other methods. The oriented crystalline growth dictated by heat transfer directions and the particular phases formed at high temperatures in the molten pool and pressures induced during the rapid solidification process will be discussed. Besides, many factors such as laser power, scan speed and cooling environments are shown to affect the laser rapid solidification rate and hence the pressures induced. With the help of experimental results, the influence of these factors on the cooling rate, pressures induced and the phases of final products are revealed.

2. Synthesis of negative thermal expansion materials by LRS

It is well known that the vast majority of materials expand on heating and contract on cooling at widely different rates. This can cause a variety of problems in applications such as delamination of layers or cracking of connections, temporary or permanent device failure due to strains induced by expansion and contraction. Materials with opposite thermal properties, namely contract on heating and expand on cooling are particularly desired to facilitate the possibility to engineer materials with controllable overall negative, zero or

positive coefficient of thermal expansion by composite them with positive thermal expansion materials. Negative thermal expansion (NTE) materials have therefore received considerable interests (Liang, 2010) since the discovery of negative thermal expansion of ZrW_2O_8 from 0.3 to 1050 K (Mary et al., 1996). However, the synthesis of negative thermal expansion materials such as ZrW_2O_8, HfW_2O_8 and etc. are quite tedious and several days or even weeks are usually needed by traditional solid state reactions or wet chemical routes. Laser rapid solidification has recently been employed for the synthesis of negative thermal expansion materials by us. Here we address the unique microstructures and special phase formation of the materials correlated with the heat transfer and pressures induced by this special technique.

2.1 Microstructures

Figs. 1a and 1b show the SEM images of the surface and cross-section of ZrW_2O_8 synthesized with 500 W laser power and 3 mm/s scan speed, respectively. It is obvious that the sample is composed of nano-threads/rods exhibiting oriented growth and distribution on both the surface and cross section. Enlarged SEM pattern (Fig. 1b) shows that the nano-threads are composed of smaller nano-crystallites. The orientation of the nanostructures reflects the directions of heat transfer since the growth of the nanostructures is against the heat flow direction.

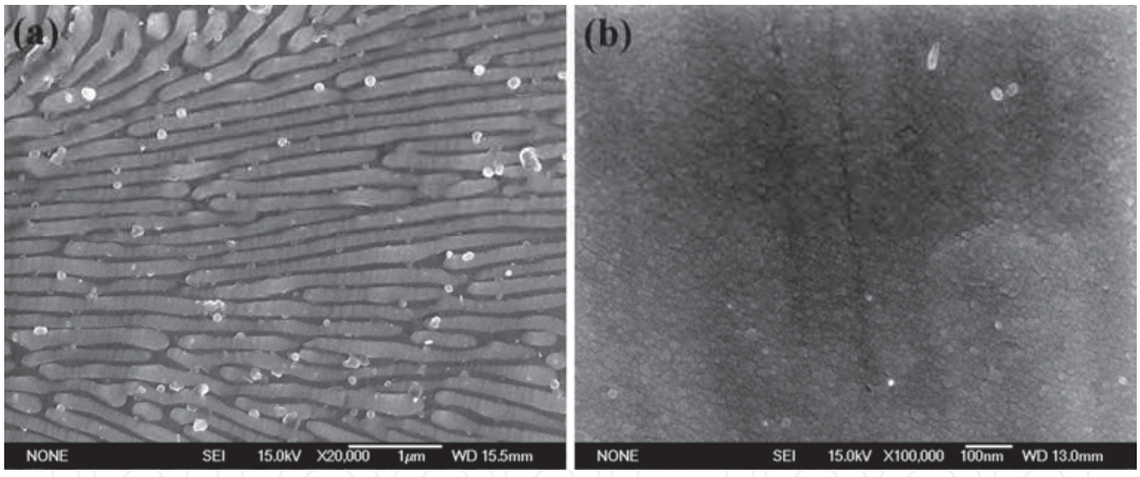

Fig. 1. SEM images of the ZrW_2O_8 block synthesized by LRS with 500 W laser power at 3 mm/s scan speed: (a) surface; (b) cross section.

The laser synthetic route is a rather rapid process, during which the raw materials are heated to melt immediately upon illumination of the laser beam and form a molten pool where the chemical reaction occurs. The product solidifies rapidly as the laser beam moves ahead. The whole process from the laser starting to illuminate to the solidification of the final product completes in only a few or tens of seconds. The heat transfer was mainly directed from the top surface to the bottom and also governed by the moving direction of the laser beam as the laser energy was absorbed by the top layer of the raw materials. The unique microstructures of the samples produced in the laser synthetic route can be attributed to the relatively oriented crystalline growth governed by heat transfer directions in the liquid droplet-like molten pool.

2.2 Pressure and compressive stress induced during LRS

Another distinct difference of the LRS with respect to solid state reactions is the pressure or stress induced in the rapid solidification process. The stress induced in the sample is proportional to solidification rate R, which is proportional to the temperature difference between the molten pool T_m and the ambient T_a, and inversely proportional to the time span Δt for the sample to cool to the final temperature (Liang et al., 2007).

$$P = AR = A\,(T_m - T_a)/\Delta t \quad (1)$$

where A is a coefficient related to the factors apart from the laser processing parameters such as the surrounding medium. Because the NTE materials expand thermodynamically on cooling, the stress induced in the rapid solidification process is compressive instead of tensile. High pressure neutron diffraction studies showed that an irreversible structural transition from α (cubic) to γ (orthorhombic) phase for ZrW_2O_8 starts at 0.21 GPa and finishes at about 0.5 GPa (Perottoni et al., 1998; Ravindran et al., 2001; Mittal et al., 2003). Eq. 1 may be tested and different phases may be synthesized by tuning the compressive stress.

In order to ensure the formation of a molten pool for sufficient reaction and rapid synthesis, T_m must equal to or higher than the highest melting point of the raw materials. Since the laser solidification is a natural process, T_a is then taken as the room temperature. According to Eq. (1), in order to decrease P, one has to decrease $\Delta T = T_m - T_a$ and to increase Δt. The compressive stress is predominately governed by the cooling rate which is closely related to laser processing parameters such as laser power, scan speed and scan mode. The most convenient and effective way to reduce the cooling rate is to increase Δt. This can be realized by reducing the scan speed since heat influence of the molten pool on the nearest solidifying part persists longer with a lower scan speed.

Figs. 2a and 2b show the Raman spectra of ZrW_2O_8 synthesized by using 800 W laser power at 6mm/s and 1mm/s scan speeds, respectively. It is clear that the γ (orthorhombic) phase dominates with 6 mm/s scan speed as revealed by the splitting of the Raman bands around 800 cm^{-1} while the α (cubic) phase appears with 1 mm/s scan speed as indicated by the presence of the character Raman bands at 904 and 934 cm^{-1} (Liang et al., 2007; 2007).

2.3 The effect of cooling in water

The surrounding medium is also expected to influence the heat transfer rate since different media has different thermal conductivities. Figs. 3a and 3b show the Raman spectra of ZrW_2O_8 synthesized by using a 500 W laser power at 3mm/s scan speed and cooled naturally in air and in water, respectively. It is obvious that the sample cooled naturally in air is dominated by the γ phase while that cooled in water exhibits both characters of α and γ phases. The appearance of the α phase in the water-cooled sample reveals that the cooling in water reduces the compressive stress of the sample.

Fig. 4 shows the SEM images of the surface and cross-section of the sample cooled in water. Compared to the microstructures of the sample cooled naturally in air (Fig. 1), the crystallites in the sample cooled in water are not so densely packed. It seems that the cooling in water produces a tensile stress which cancels the compressive stress, leads to plentiful micro-cracks and loosens the structure. The α phase formation can be understood by the canceling of the compressive stress.

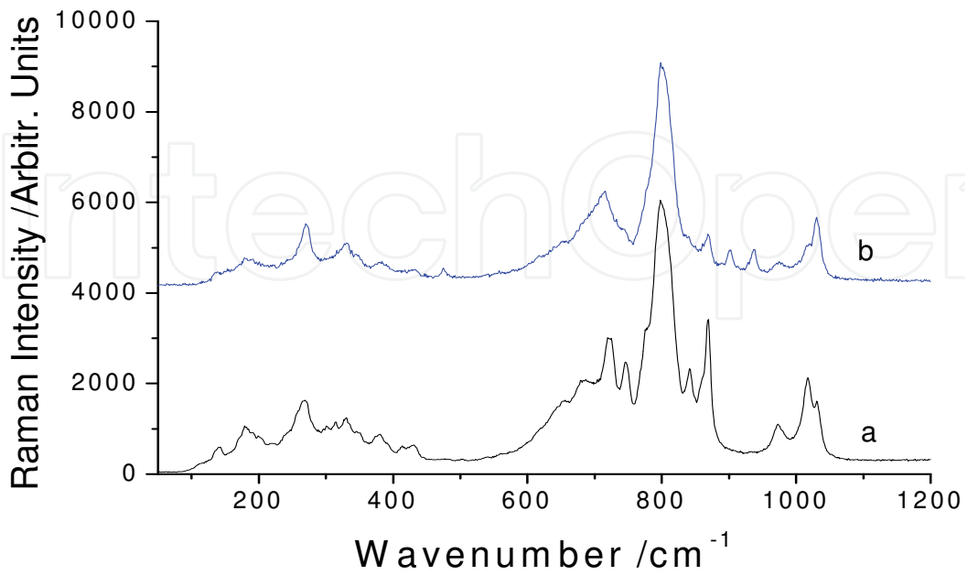

Fig. 2. Raman spectra of ZrW_2O_8 synthesized with 800 W laser power and different scan speed: (a) 6 mm/s and (b) 1 mm/s.

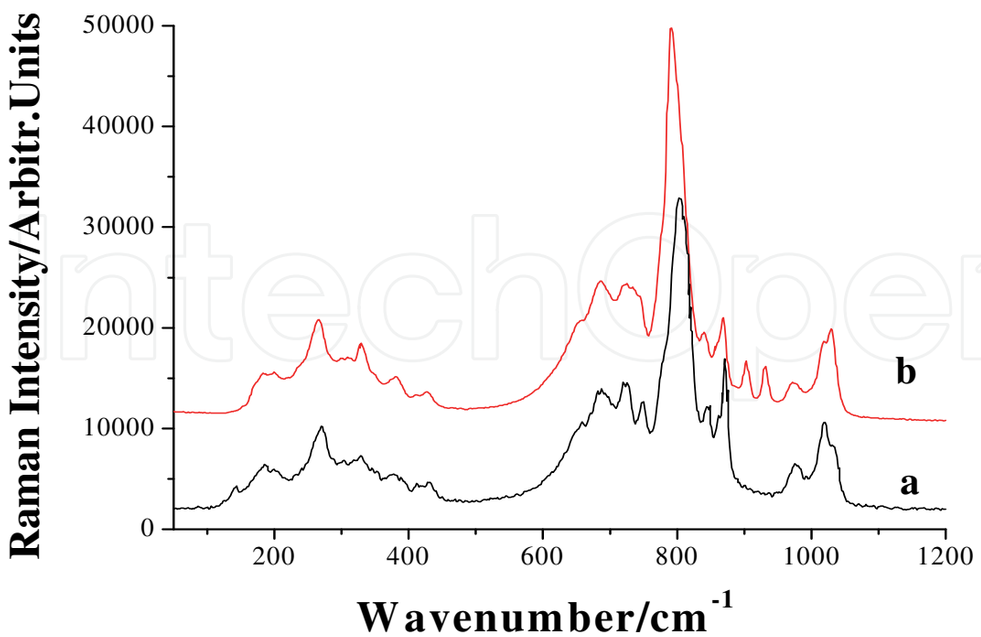

Fig. 3. Raman spectra of ZrW_2O_8 synthesized with 500 W laser power and 3 mm/s scan speed cooled (a) in air and (b) in water.

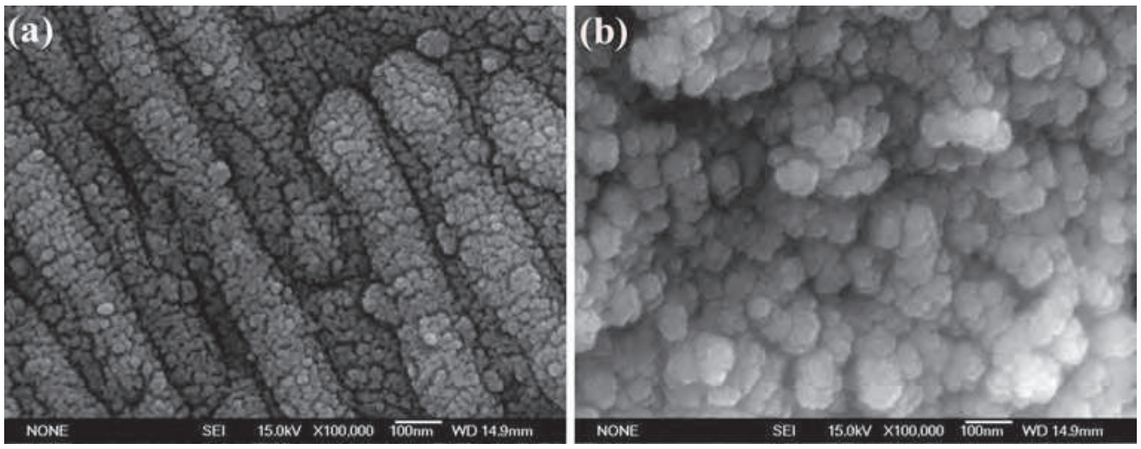

Fig. 4. SEM images of the ZrW_2O_8 block synthesized by LRS and cooled in water.

Fig. 5 shows the mass ratio of the γ to α phase with 500 W and 600 W laser power at different scan speeds, respectively. The content of the γ phase show a general increases while that of the α phase decreases with increasing the scan speed. Since the γ phase can only be produced under pressures ≥ 0.21 GPa, the increase in the γ phase content with scan speed confirms that the compressive stress increases with cooling rate. Besides, at higher scan speed (≥2mm/s), a higher laser power results in a lower content of the γ phase. A higher laser power may result in higher temperatures in the molten pool, but at the same time more heat will be transferred to the part behind which slows the cooling rate of the solidifing part. This leads to a lower compressive stress and consequently lower content of the γ phase. However, the situation is reversed at lower scan speed (1mm/s), i. e. the lower the laser power is, the lower the content of the γ phase generates. The temperature increasing in the molten pool with laser power seems to play a more important role at lower scan speed, resulting in a higher content of the γ phase with higher laser power.
HfW_2O_8 can also be synthesized by LRS. The optimum synthesis conditions for HfW_2O_8 was shown to be around 700 W laser power and 1 mm/s scan speed. These requirements are much stricter than those for the synthesis of ZrW_2O_8 due to the higher melting point of HfO_2 than that of ZrO_2. It is deduced that the pressure induced in the solidification process for the synthesis of HfW_2O_8 is around 0.6 GPa since the sample is dominated by α phase with only minor content of γ phase (Liang et al., 2007). Besides ZrW_2O_8 and HfW_2O_8, NTE materials of $Y_2W_3O_{12}$ and $Y_2Mo_3O_{12}$ can also be synthesized by LRS (Liang et al., 2008; Yuan et al., 2009).

3. Synthesis of ion conductive perovskite oxides by LRS for SOFC applications

Solid oxide fuel cells (SOFCs) can directly convert chemical energy of fuels to electrical energy with advantages of high electrical efficiency, fuel versatility and low pollution emissions. The perovskite oxide, strontium- and magnesium-doped $LaGaO_3$ (LSGM), exhibits a higher ionic conductivity than the conventional Y_2O_3-stabilized ZrO_2 electrolytes over a wide range of oxygen partial pressure. This makes $LaGaO_3$-based oxides the most promising candidates as electrolytes for intermediate temperature SOFCs. However, the synthesis of a pure single phase material of LSGM is a rather difficult task. For example, the solid state reactions suffer from severe time and energy wasting while the wet chemical methods require expensive metal alkoxide precursors, great care in mixing the precursors to

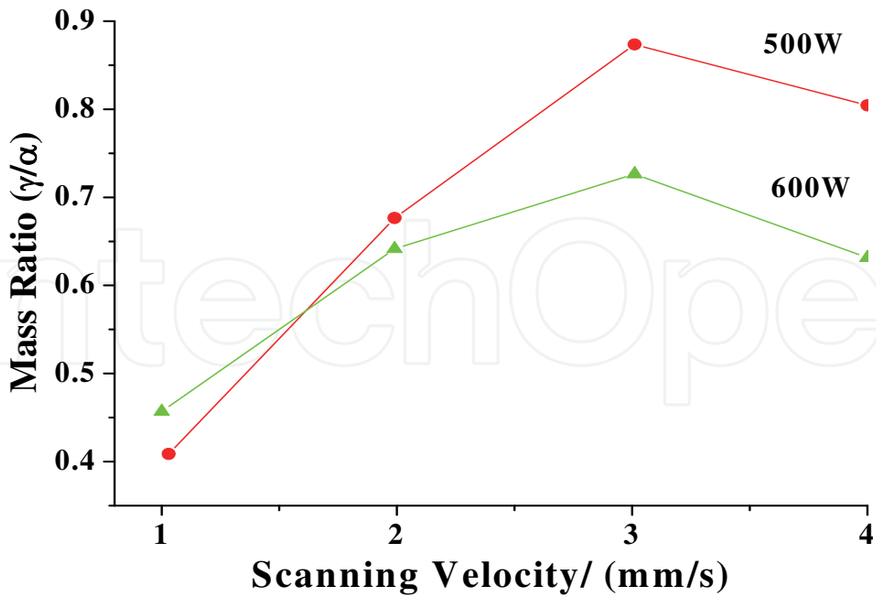

Fig. 5. The mass ratio of the γ to α phase at different scan speeds.

achieve the desired stoichiometry and tedious pretreatment before the final calcinating step. Due to the narrow composition range for the stability of the perovskite phase, small deviations from the ideal composition would result in secondary phases which deteriorate the performance of the electrolyte. We have recently demonstrated that the LRS technique can be used to the synthesis of $La_{0.9}Sr_{0.1}Ga_{0.8}Mg_{0.2}O_{3-\delta}$ (LSGM) (Zhang et al., 2010) and $La_{0.8}Sr_{0.2}Ga_{0.83}Mg_{0.17-x}Co_xO_{2.815}$ with x=0, 0.05, 0.085, 0.10 and 0.15, respectively.

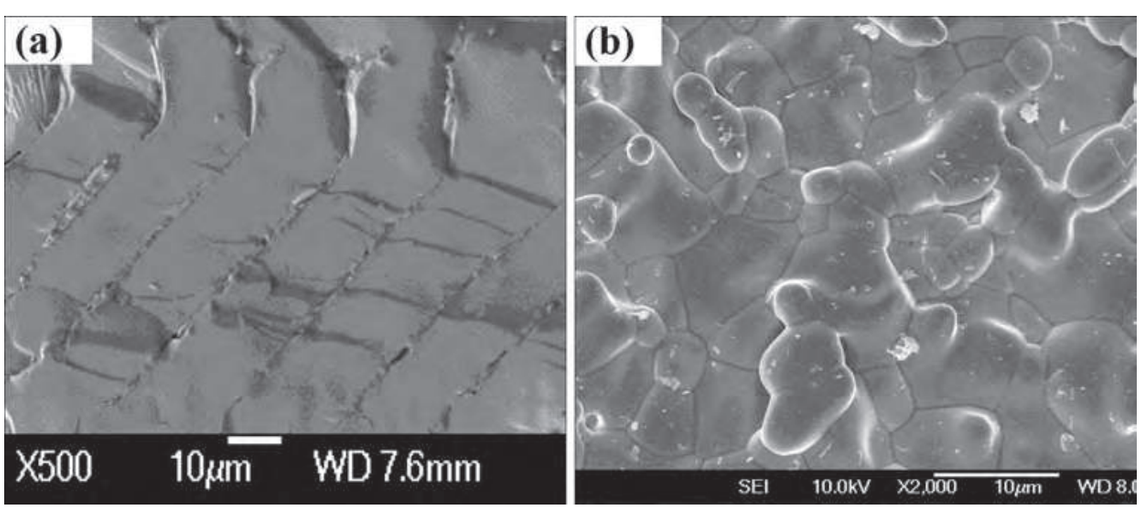

Fig. 6. SEM images of the LSGM samples prepared by (a) LRS and (b) solid state reactions at 1600 °C.

Figs. 6a and 6b show the typical SEM images of the fractured cross-sections of $La_{0.9}Sr_{0.1}Ga_{0.8}Mg_{0.2}O_{3-\delta}$ (LSGM) samples prepared by LRS and solid state reactions, respectively. It is evident that the microstructure of the sample by LRS is characterized by

relative orderly arranged and densely packed blocks while that prepared by solid state reactions consists of densely packed irregular shaped globose grains. The unique microstructures of the samples produced in the laser synthetic route are attributed to the relatively oriented crystalline growth governed by heat transfer directions.

Although both samples have similar density (98.5 % by LRS and 96.9% by SSR), the sample prepared by LRS exhibits much superior conductivities (0.027, 0.079 and 0.134 Scm^{-1} obtained at 600, 700 and 800 °C) to the sample prepared by solid state reactions (0.019, 0.034 and 0.041 Scm^{-1}) (Zhang et al., 2010). Both XRD analysis and Raman spectroscopic study suggest that the sample prepared by LRS crystallized in an orthorhombic and that by solid state reactions in a monoclinic phase.

The samples $La_{0.8}Sr_{0.2}Ga_{0.83}Mg_{0.17-x}Co_xO_{2.815}$ with high purity were also prepared by LRS. It is shown that that Co-doped LSGMs exhibit unique spear-like or leaf-like microstructures (not shown here) and superior oxide ion conductivity. The electrical conductivities of $La_{0.8}Sr_{0.2}Ga_{0.83}Mg_{0.085}Co_{0.085}O_{2.815}$ are measured to be 0.067, 0.124 and 0.202 Scm^{-1} at 600, 700 and 800°C, respectively, being much higher than those of the same composition by solid state reactions (0.026, 0.065, 0.105 Scm^{-1}).

The unique microstructures of the samples prepared by LRS should account mainly for their superior electrical properties to those of the samples prepared by solid state reactions. The relatively oriented and densely packed ridge-like (for LSGM) or leave-like (Co-doped LSGM) grains with large and regular sizes in the samples by LRS greatly reduce the scattering probabilities and thus increase the mean free path or the mean free time of charge carriers during the drift motion.

It can be speculated from the appearances and SEM images that the starting materials were sufficiently molten in the molten pool. Since the melting points of the raw materials La_2O_3, $SrCO_3$, Ga_2O_3 and MgO are about 2315, 1497, 1740 and 2827°C, respectively, the temperature of the molten pool is expected to be above 2830°C. The sufficiently high temperature ensured sufficient melting of the raw materials and consequently rapid and uniform reactions.

4. Conclusion

LRS has been used to the synthesis of NTE and oxide ion conductive materials for SOFCs. Special characters of the LRS are the directed heat transfer and rapid solidification. The heat transfer is mainly directed from the top surface to the bottom and also governed by the moving direction of the laser beam as the laser energy is absorbed by the top layer of the raw materials. The samples synthesized by LRS exhibits usually unique microstructures which can be attributed to the relatively oriented crystalline growth governed by heat transfer directions in the liquid droplet-like molten pool. It is also shown that a compressive stress induced in the rapid solidification process can be large enough for the generation of the γ phase ZrW_2O_8. Due to the rapid solidification from the molten pool, highly densely-packed blocks of the samples can be easily achieved, in contrast to traditional solid state reactions where sintering additives are usually required to achieve high density of samples. The densely packed unique microstructures and perhaps also the spectial phases of the electrolyte samples prepared by LRS make them superior in electrical properties to those of the samples prepared by solid state reactions.

5. Acknowledgment

This work was supported by the National Science Foundation of China (No. 10974183)

6. References

Chao, M. J. & Liang E. J. (2004). Effect of TiO_2-doping on the microstructure and the wear properties of laser-clad nickel-based coatings, *Surf. Coat. Techn.* Vol. 179, No. 2-3, (Febrary, 2004), pp. 265-271, ISSN 0257-8972

Bogue, R. (2010). Fifty years of the laser: its role in material processing, *Assembly Automation*, Vol. 30, No. 4, (April, 2010), pp. 317-322, ISSN 0144-5154

Kruusing A, Underwater and water-assisted laser processing:Part 1—general features, steam cleaning and shock processing, *Optics and Lasers in Engineering*, Vol. 41, No. 2, (Febrary, 2004) pp. 307-327, ISSN: 0143-8166

Liang, E.J.; Wu, T. A.; Yuan, B.; Chao, M. J. & Zhang, W. F. Synthesis, microstructure and phase control of zirconium tungstate with a CO2 laser, *J Phys D Appl Phys*.Vol. 40, No. 10, (May, 2007), pp. 3219-3223, ISSN: 0022-3727; Liang, E. J.; Wang, S. H.; Wu, T. A.; Chao, M. J.; Yuan, B. & Zhang, W. F. Raman spectroscopic study on structure, phase transition and restoration of zirconium tungstate blocks synthesized with a CO_2 laser, *J Raman Spectrosc,*Vol. 38, No. 9, (September, 2007) , pp. 1186-1192, ISSN: 0377-0486; Liang, E. J.; Wang, J. P.; Xu, E. M.; Du, Z. Y. & Chao, M .J. Synthesis of hafnium tungstate by a CO_2 laser and its microstructure and Raman spectroscopic study, *J Raman Spectrosc.*, Vol 39, No. 7, (July, 2008), pp. 887-892.; Liang, E. J.; Huo, H. L.; Wang, Z.; Chao, M .J. & Wang, J. P. Rapid synthesis of $A_2(MoO_4)_3$ ($A=Y^{3+}$ and La^{3+}) with a CO_2 laser, *Solid State Sci*., Vol. 11, No. 1, (January,2009), pp. 139-143, ISSN: 1293-2558 ; Liang, E. J.; Huo, H. L. & Wang, J. P. Effect of water species on the phonon modes in orthorhombic $Y_2(MoO_4)_3$ revealed by Raman spectroscopy, *J Phys Chem C*, Vol. 112, No. 16, (April, 2008), pp. 6577-6581, ISSN:1932-7447; Liang, E. J. Negative Thermal Expansion Materials and Their Applications : A Survey of Recent Patents, *Recent Patents on Mat Sci.,*Vol. 3, No. 2, (May, 2010), pp. 106-128, ISSN:1874-4648

Mary, T. A.; Evans, J. S. O.; Vogt, T. & Sleight, A. W. Negative thermal expansion from 0.3 to 1050 Kelvin in ZrW2O*8*, *Science*, Vol. 272, No. 5258, (April, 1996), pp. 90-92, ISSN: 0036-8075

Mittal, R.; Chaplot, S. L.; Kolesnikov, A. I.; Loong, C. K. & Mary, T. A. Inelastic neutron scattering and lattice dynamical calculations of negative thermal expansion in ZrW_2O_8, *Phys. Rev. B*, Vol.68 No. 5, (August, 2003), pp. 054302, ISSN: 1098-0121

Perottoni, C. A. & da Jornada J A. H.,Pressure induced amorphization and negative thermal expansion in ZrW_2O_8, *Science*, Vol. 280, No. 5365, (May, 1998), pp. 886-889, ISSN: 0036-8075

Ravindran, T. R.; Arora. A. K. & Mary, T A. High-pressure Raman spectroscopic study of zirconium tungstate, *J. Phys: Cond. Matter*, Vol 13, No. 50, (December, 2001), pp. 11573-11588, ISSN: 0953-8984

Wang, D. S.; Liang, E. J.; Chao, M. J. & Yuan, B. Investigation on the Microstructure and Cracking Susceptibility of Laser-Clad V2O5/NiCrBSiC Coatings, Surf. Coat. Techn. Vol. 202, No. 8. (January, 2008), pp. 1371-1378, ISSN 0257-8972

Yuan, C. ; Liang, Y. ; Wang, J. P. & Liang, E. J. Rapid Synthesis and Raman Spectra of Negative Thermal Expansion Material Yttrium Tungstate, *J Chin Ceram Soc*., Vol 37, No. 5, (May, 2009), pp. 726-732, ISSN: 0454-5648

Zhang, J.; Liang, E. J. & Zhang, X. H. Rapid synthesis of $La_{0.9}Sr_{0.1}Ga_{0.8}Mg_{0.2}O_{3-\delta}$ electrolyte by a CO2 laser and its electric properties for intermediate temperature solid state oxide fuel cells, *J. Power Sources*, Vol. 195, No. 19, (October, 2010), 195: 6758-6763, ISSN:0378-7753

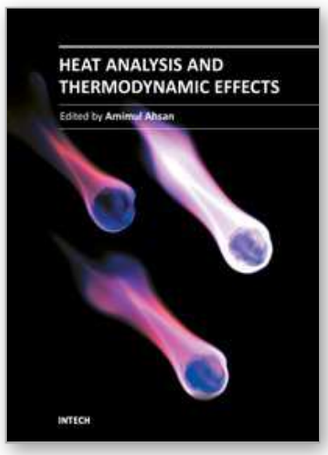

Heat Analysis and Thermodynamic Effects
Edited by Dr. Amimul Ahsan

ISBN 978-953-307-585-3
Hard cover, 394 pages
Publisher InTech
Published online 22, September, 2011
Published in print edition September, 2011

The heat transfer and analysis on heat pipe and exchanger, and thermal stress are significant issues in a design of wide range of industrial processes and devices. This book includes 17 advanced and revised contributions, and it covers mainly (1) thermodynamic effects and thermal stress, (2) heat pipe and exchanger, (3) gas flow and oxidation, and (4) heat analysis. The first section introduces spontaneous heat flow, thermodynamic effect of groundwater, stress on vertical cylindrical vessel, transient temperature fields, principles of thermoelectric conversion, and transformer performances. The second section covers thermosyphon heat pipe, shell and tube heat exchangers, heat transfer in bundles of transversely-finned tubes, fired heaters for petroleum refineries, and heat exchangers of irreversible power cycles. The third section includes gas flow over a cylinder, gas-solid flow applications, oxidation exposure, effects of buoyancy, and application of energy and thermal performance index on energy efficiency. The forth section presents integral transform and green function methods, micro capillary pumped loop, influence of polyisobutylene additions, synthesis of novel materials, and materials for electromagnetic launchers. The advanced ideas and information described here will be fruitful for the readers to find a sustainable solution in an industrialized society.

How to reference
In order to correctly reference this scholarly work, feel free to copy and paste the following:

E. J. Liang, J. Zhang and M. J. Chao (2011). Synthesis of Novel Materials by Laser Rapid Solidification, Heat Analysis and Thermodynamic Effects, Dr. Amimul Ahsan (Ed.), ISBN: 978-953-307-585-3, InTech, Available from: http://www.intechopen.com/books/heat-analysis-and-thermodynamic-effects/synthesis-of-novel-materials-by-laser-rapid-solidification

INTECH
open science | open minds

InTech Europe
University Campus STeP Ri
Slavka Krautzeka 83/A
51000 Rijeka, Croatia
Phone: +385 (51) 770 447
Fax: +385 (51) 686 166
www.intechopen.com

InTech China
Unit 405, Office Block, Hotel Equatorial Shanghai
No.65, Yan An Road (West), Shanghai, 200040, China
中国上海市延安西路65号上海国际贵都大饭店办公楼405单元
Phone: +86-21-62489820
Fax: +86-21-62489821

IntechOpen